



Molecular dynamic study on structural and dynamic properties of water, counter-ions and polyethylene glycols in Na-montmorillonite interlayers

Mingshan Zhang^a, Hui Mao^{b,c}, Zhehui Jin^{a,*}

^a School of Mining and Petroleum Engineering, Department of Civil and Environmental Engineering, University of Alberta, Edmonton, AB T6G 1H9, Canada

^b State Key Laboratory of Oil and Gas Reservoir Geology and Exploitation, Chengdu University of Technology, Chengdu, Sichuan 610059, China

^c College of Energy Resources, Chengdu University of Technology, Chengdu, Sichuan 610059, China

ARTICLE INFO

Keywords:

Molecular dynamics simulation
Montmorillonite clay
Clay interlayer
Polyethylene glycols
Counter-ions

ABSTRACT

Understanding the interfacial behavior of PEGs and water-PEG interaction in montmorillonite (MMT) interlayer is of great importance to the design of high-performance drilling fluids. In this work, we apply molecular dynamic (MD) simulations to study the structural properties of three low molecular weight PEGs (PEG2, PEG4 and PEG8) in MMT interlayers. We found that PEG2 incline to be parallel to the MMT surfaces, while PEG4 molecules tend to form a crown-like structure, hosting Na⁺ ions within. PEG8 molecules likely adopt helical or coil configurations caging Na⁺ inside. Thanks to the wrapping and caging effect, hydration ability of Na⁺ ion is significantly reduced. Moreover, at a higher concentration with PEG4 and PEG8, more Na⁺ ions are trapped in the middle of the pore due to the PEG caging. As PEG concentration increases, some water molecules are displaced from the pore surface. As a result, the hydrogen bonding number between water and pore surface decreases. Furthermore, the diffusion coefficients of water and Na⁺ ions are suppressed in the presence of PEGs. Our study provides important insights into the structural properties of water, counter-ions, and PEG molecules in MMT interlayers and the optimization of high-performance drilling fluids.

1. Introduction

As one of the most common minerals in the strata, clay is one type of layered materials [1,2]. Polymer adsorption in clay interlayers is of fundamental importance for many engineering applications, such as geological storage of toxic and radioactive wastes [3–5], oil recovery enhancement [6], nanocomposite [7–9], and additives in water-based drilling fluids (WBDFs) [10–16], which have been widely employed to drill oil/gas wells due to their low toxicity and excellent performance [16–21]. Montmorillonite (MMT), a common clay mineral, consists of stacks of negatively charged layers, neutralized by Na⁺ or Ca²⁺ cations [22–25]. The exchangeable counter-ions and charged MMT surfaces can attract water molecules, resulting in clay hydration and swelling [26–28]. During oil/gas exploration and production, clay swelling may induce borehole instability, which can significantly increase drilling costs [19,29–33]. To develop high-performance drilling fluids, polyethylene glycols (PEGs), which are environmentally friendly and biodegradable [11,34], have been introduced into WBDFs to effectively minimize clay swelling [10,11,15,16]. There are several proposed mechanisms about clay swelling inhibition due to PEGs: 1) PEG molecules diffuse into the MMT interlayers and spontaneously displace water

molecules [29,35]; 2) Adsorbed PEG molecules disrupt the hydrogen bonding between water molecules and clay surfaces, while they form hydrogen bonding with clay surfaces [36,37]; 3) PEG molecules may disturb water hydration around counter-ions [37]. Therefore, the knowledge about the structural and dynamic properties of water, counter-ions, and PEG molecules in MMT interlayers can provide key insights into the swelling inhibition mechanisms and optimization of drilling fluids.

There have been several experimental studies of structural properties of PEGs in clay minerals [8,35,38–42]. Parfitt *et al.* [35] measured the adsorption isotherms of various PEGs with molecular weight ranging from 200 to 20,000 in MMT saturated with various counter-ions at 275 and 298 K. They found that as PEG molecular weight increases, the free energies of adsorption become more negative, while entropy changes become increasingly positive. Aston *et al.* [37] investigated the effect of glycol additives on shale physical properties such as dispersion, swelling and hardness. They observed that glycol additives can displace water from clay, indicating a stronger affinity for glycol with clay surface than that for water. Su *et al.* [42] investigated PEO adsorption on various smectites and reported that the hydrophobic interaction between -CH₂- groups and siloxane surface of clay is the major driving

* Corresponding author.

E-mail address: zhehui2@ualberta.ca (Z. Jin).

<https://doi.org/10.1016/j.apsusc.2020.147700>

Received 28 February 2020; Received in revised form 17 August 2020; Accepted 26 August 2020

Available online 04 September 2020

0169-4332/ © 2020 Elsevier B.V. All rights reserved.

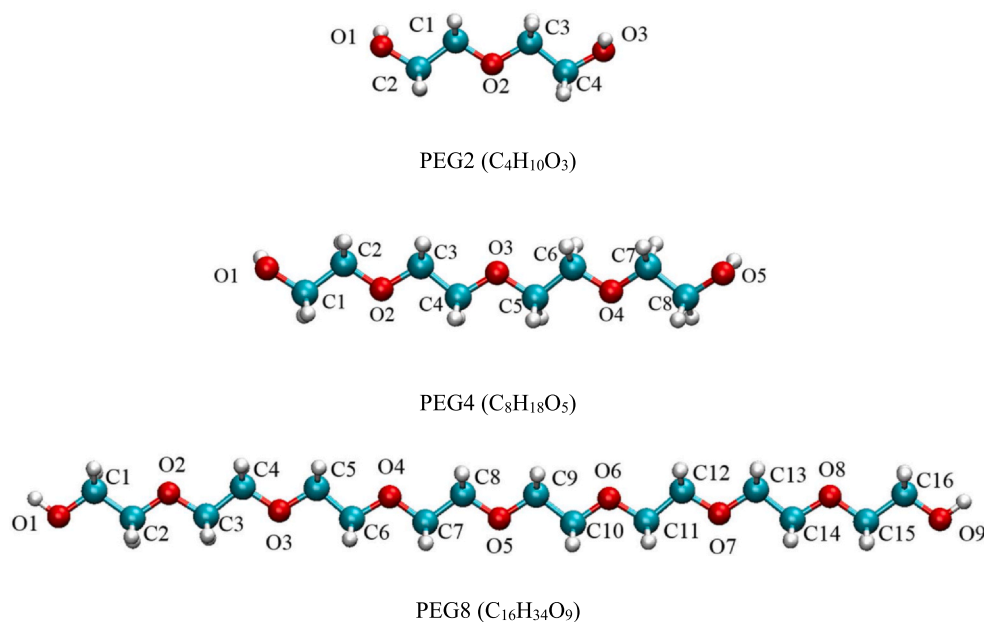


Fig. 1. Molecular structures and formula of PEGs with different molecular weights. Color scheme: white, H; red, O; cyan, C. (For interpretation of the references to color in this figure legend, the reader is referred to the web version of this article.)

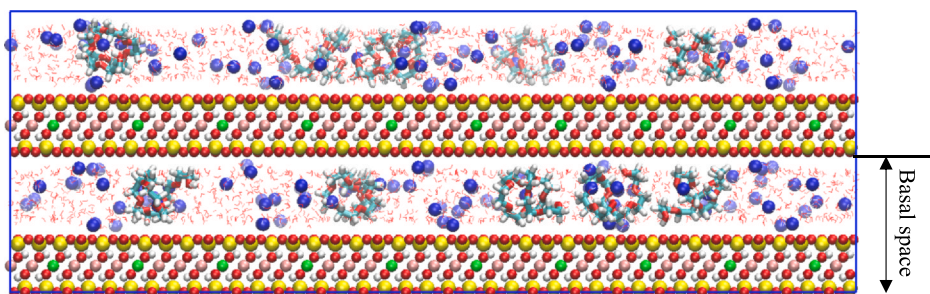


Fig. 2. Snapshot of the equilibrated MMT interlayer filled with water of 0.3 g/clay g and 4 wt% PEG8 with a d -spacing of 17.5 Å. Color scheme: yellow, Si; green, Al; red, O; white, H; blue, Na; pink, Mg; cyan, C. The blue line frame represents the box boundary. (For interpretation of the references to color in this figure legend, the reader is referred to the web version of this article.)

force for PEO adsorption on smectite. De Souza *et al.* [40] studied the adsorption behavior of PEGs with a wide range of molar mass by XRD and thermogravimetric analysis. It is assumed that PEG molecules can be adsorbed on clay surface by competing with the water molecules to stabilize shale cuttings. Aranda *et al.* [43] investigated PEO intercalation into 2:1 charged phyllosilicates. They proposed that PEOs may adopt helical conformations in the interlayer region wrapping counterions to form a Na^+ -PEO complex. While these measurements provided important insights into PEG adsorption on clay surface and inhibition mechanism, experimental measurements are unable to elucidate the structural and dynamic properties of MMT interlayer species from molecular perspectives.

Computer simulation has been proven as a promising technique to investigate structural and dynamic properties of clay-water systems from an atomistic level [24,25,44–48]. The microscopic structures of PEG adsorption on clay basal surfaces have been reported [29,33,49–52]. Bains *et al.* [29] used grand canonical Monte Carlo (GCMC) and molecular dynamic (MD) simulations to study the inhibition mechanism of clay swelling by PEG300 at 300 K. They indicated that PEG molecules in clay interlayers can incur water desorption, resulting in a reduced clay swelling tendency. However, they used rigid PEG molecules, while ignoring their flexibility. Suter *et al.* [33] simulated clay-PEG systems by removing water molecules step-by-step at

300 K and quantified hydration energies at various water contents. They suggested that low molecular weight or low concentration of PEG is required for effective clay swelling inhibition. Anderson *et al.* [49] used MD simulations to investigate the interaction between PEG with molecular weight of 414 and MMT at 300 K. They did not observe the evidence of hydrogen-bond interaction between the PEG alcohol groups and clay tetrahedral O atoms, indicating that in the presence of water and counter-ions, PEG molecules are unlikely to adsorb strongly at the clay surface. To some extent, these previous studies can partially implicate the swelling inhibition mechanisms, but they did not reveal the structural and dynamic properties of clay interlayer species in relation to clay swelling.

Therefore, in this work, we explicitly study the structural and dynamic properties of water, counter-ions, and PEG molecules with varying chain lengths and concentrations in MMT interlayers at 300 K and 1 atm by using MD simulations. PEGs with molecular weight greater than or equal to 200 g/mol have been used for wellbore stability [53]. In fact, PEGs used in WBDFs consist of a mixture of various PEG species. Thus, three different PEG molecules with carbon numbers of 2 (PEG2), 4 (PEG4), 8 (PEG8) are chosen as the target candidates in this work. We also evaluate the effect of PEGs on interfacial and mobility properties of water and counter-ions, which are Na^+ ions in this work. The hydration behavior of Na^+ ion in the presence of PEGs and water is

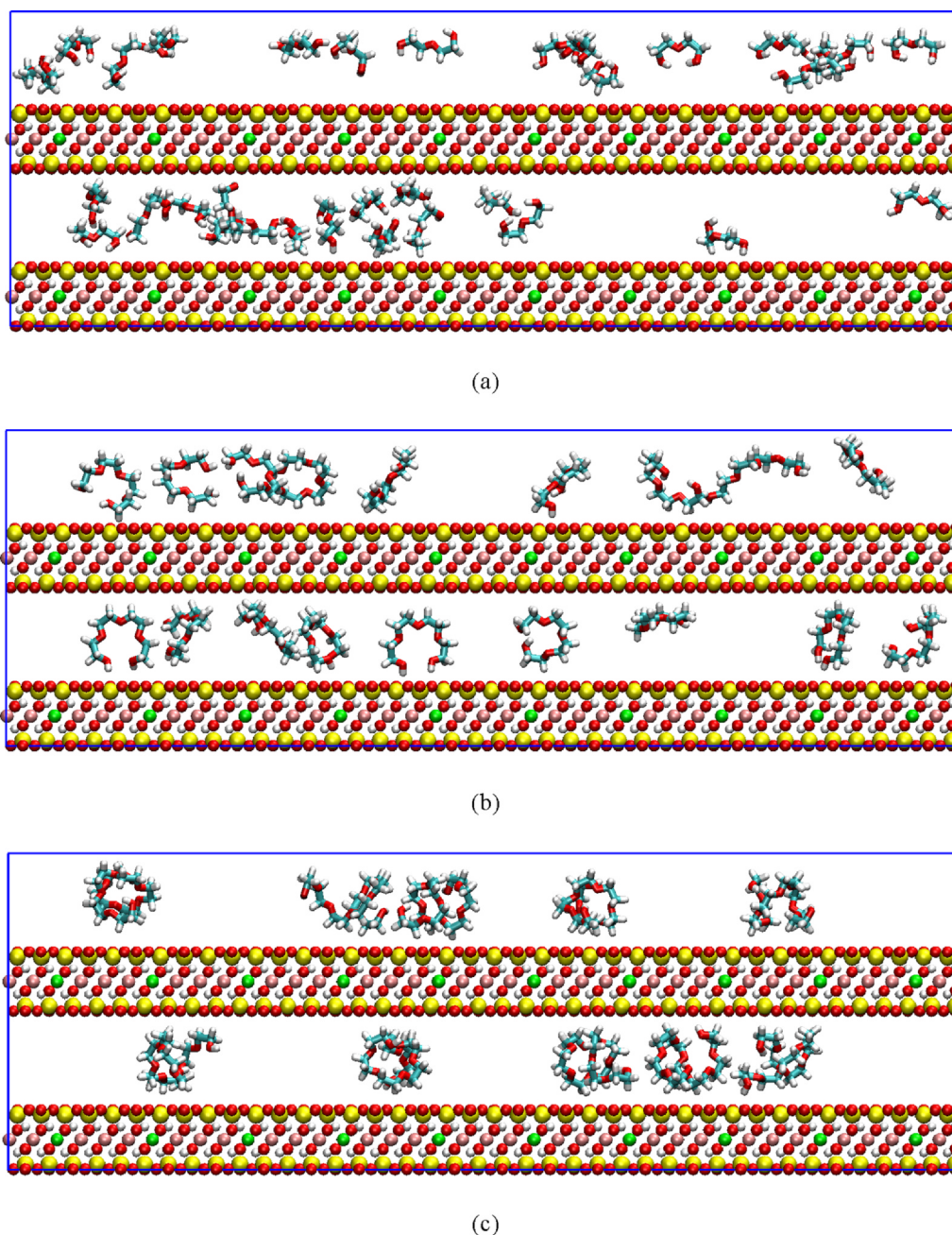


Fig. 3. Snapshots of the equilibrated systems with 4 wt% (a) PEG2; (b) PEG4; (c) PEG8 in MMT interlayers at 300 K. For clarity, we omit the water molecules and Na^+ ions. The color scheme is the same as in Fig. 1.

demonstrated. We found that PEGs with varying chain lengths exhibit various configurations when intercalated into MMT interlayers. The introduction of PEGs lowers diffusion coefficients of water as well as Na^+ ion. Furthermore, Na^+ ion hydration ability is significantly suppressed when they are surrounded by PEG4 and PEG8 molecules. Our work should provide important insights into the performance of PEGs in MMT interlayers and shed some lights onto the clay swelling inhibition mechanism by PEGs.

This paper is organized as follows. In Section 2, we introduce the molecular models and simulation methods. In Section 3, we analyze the adsorption behavior of interlayer species, hydrogen bond, diffusion coefficients of water and Na^+ ions, and Na^+ ion hydration behavior. In Section 4, we summarize the key conclusions and discuss the potential implications.

2. Molecular model and simulations

2.1. Molecular models

All MD simulations are carried out with LAMMPS package [54]. Wyoming-type montmorillonite of unit cell formula $\text{Na}_{0.75}(\text{Si}_{7.75}\text{Al}_{0.25})(\text{Al}_{3.5}\text{Mg}_{0.5})\text{O}_{20}(\text{OH})_4$ is used to model the MMT substrate [25,45]. The model system consists of two clay sheets, each consists of $20 \times 10 \times 1$ crystallographic unit cells with a dimension of $105.6 \text{ \AA} \times 91.4 \text{ \AA} \times 6.56 \text{ \AA}$. The molecular structure and formula of PEGs used in this work are shown in Fig. 1. It is suggested that 3 wt%–10 wt% PEGs are commonly used during drilling operation [31,39]. We add 4 wt%, 8 wt%, and 12 wt% PEGs to the system with 4800 H_2O molecules (corresponding to water content as 0.3 g/clay g) to investigate the effect of PEG concentration. The number of various PEGs employed in the

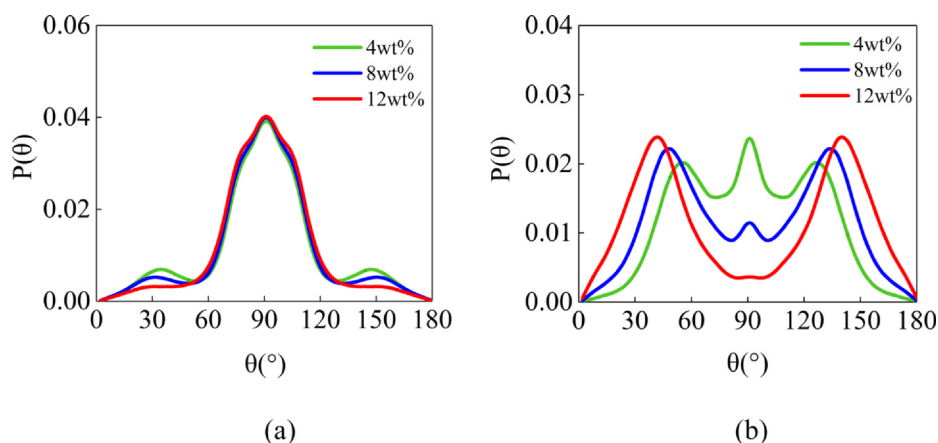


Fig. 4. Angle distributions of (a) PEG2; (b) PEG4 for various concentrations.

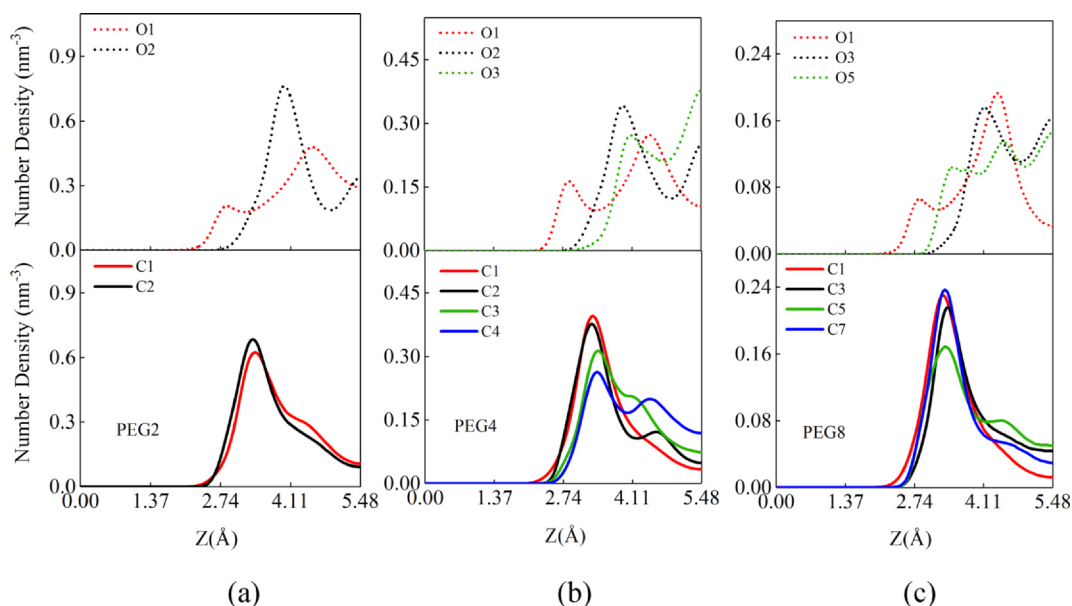


Fig. 5. Density profiles of C and O atoms of (a) PEG2; (b) PEG4; (c) PEG8 for 4 wt% at 300 K. $Z = 0$ represents the position of outmost tetrahedral O for all the simulation system.

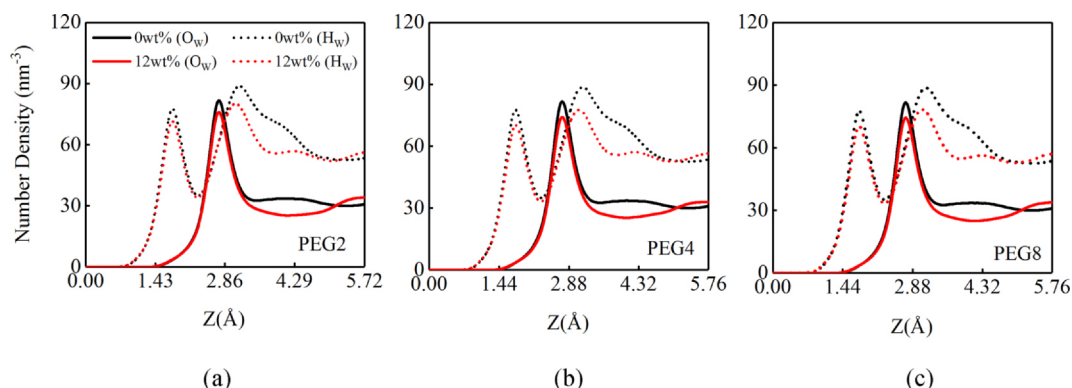


Fig. 6. Density profiles of O_w (solid line) and H_w (short dot line) in the presence of (a) PEG2; (b) PEG4; (c) PEG8.

simulations is listed in Table S1.

2.2. Force fields

The Lennard-Jones and partial charge parameters of MMT are taken from the CLAYFF force field [55] which can accurately reproduce

structural and spectroscopic properties of clays as well as dynamical and energetic properties of clay interlayers and aqueous interfaces [44,46,48,50,51]. Flexible simple point charge (SPC) model [56] is applied to simulate water molecules. Na^+ ions are simulated by using the parameters from Smith *et al.* [57]. These force fields have been proven to be compatible with each other. The OPLS-AA force field [58]

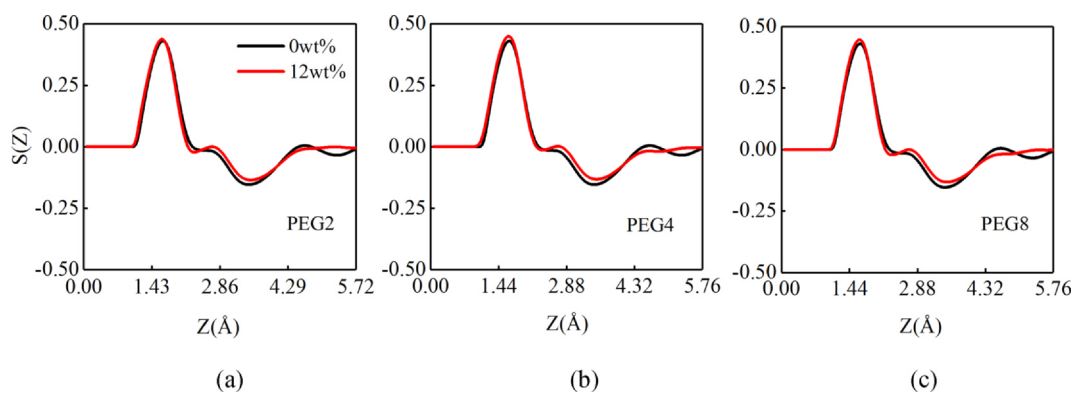


Fig. 7. $S(Z)$ of water molecules in the presence of (a) PEG2; (b) PEG4; (c) PEG8.

which has shown an excellent performance for modeling organic molecules is adopted to simulate PEG molecules. Extensive examples of the combination of CLAYFF and OPLS-AA have been reported to investigate the interactions between organic molecules and clay minerals [51,59–61].

The interactions between atoms are modeled as pairwise additive potentials including Lennard-Jones (LJ) 12-6 and coulomb potentials,

$$V(r_{ij}) = 4\epsilon_{ij} \left[\left(\frac{\sigma_{ij}}{r_{ij}} \right)^{12} - \left(\frac{\sigma_{ij}}{r_{ij}} \right)^6 \right] + \frac{q_i q_j}{4\pi\epsilon_0 r_{ij}} \quad (1)$$

where r_{ij} , σ_{ij} , and ϵ_{ij} , q_i are the separation distance, LJ well depth, and LJ size, the partial charge of atom i , respectively. The Lorentz–Berthelot mixing rule [62] is used to calculate interactions between atoms with different LJ parameters. The non-bond interactions are truncated at a distance of 12 Å with shift. The long-range electrostatic interactions are treated with the particle-particle particle-mesh (PPPM) method [63] with a precision value of 10^{-4} . Three-dimensional periodic boundary conditions are applied to the simulation cell.

2.3. Simulation details

First, we validate our model by calculating the basal spacing of Na-MMT with different water contents in the absence of PEG using the NP_zT ensemble [25,45,46,48] (i.e., with a fixed number of molecules, a constant pressure in the z -direction normal to the clay substrates, and a constant temperature) at 300 K and 1 atm. The interlayer spacing distances with varying water contents show an excellent agreement with previous simulations and experiments [25,26,46,48,64–66] as shown in Table S2.

After the calibration, we simulate the system without PEG (i.e. 0 wt%), and then water molecules and Na^+ ions altogether with PEG molecules are introduced into the simulation box.

Firstly, we applied the NP_zT ensemble for 1.5 ns to obtain the equilibrium basal spacings for various PEG concentrations as shown in Table S3. We find that the basal spacing increases as more PEG molecules are intercalated into the MMT interlayers. The system is then equilibrated by the NVT (constant number of particles, volume and temperature) ensemble by keeping the MMT sheets fixed for 20 ns (from $t = 0$ to $t = 20$ ns), followed by 10-ns production runs (from $t = 20$ ns to $t = 30$ ns) for data analysis. A snapshot of MD-equilibrated system presented by VMD package [67] with 4 wt% PEG8 is shown in Fig. 2. System temperature is maintained by the Nošé–Hoover thermostat [68] using a relaxation time of 0.1 ps. The equations of motion are integrated by the Verlet algorithm [69] with a time step of 1 fs with an interval of 0.02 ps to collect statistics data and the interval for recording trajectories is 0.3 ps.

Atomic trajectories of 600-ps NVT simulation are stored every 0.3 ps for Na^+ ion and water diffusion analysis. Two-dimensional self-diffusion coefficients in the x - y plane (D_{xy}) are calculated from the

mean-square displacement (MSD) according to the Einstein equation [70],

$$D_{xy} = \frac{1}{4Nt} \sum_{i=1}^N \langle |\vec{r}_i(t) - \vec{r}_i(0)|^2 \rangle \quad (2)$$

where N is the number of molecules, $\vec{r}_i(t)$ is the center-of-mass position of the i -th molecule at time t , $\vec{r}_i(0)$ is the center-of-mass position of the i -th molecule at time 0. To minimize the error, D_{xy} is calculated based on the data between 150 and 400 ps [71].

3. Results and discussion

We calculate the distribution of various interlayer species including PEGs, water and Na^+ ions and analyze the diffusion coefficients of water and Na^+ ions. In the end, we discuss the Na^+ ion hydration behavior in the presence of PEGs.

3.1. Distribution and structural properties of interlayer species

3.1.1. Polyethylene glycols

Snapshots of the equilibrated systems with 4 wt% PEG2, PEG4 and PEG8 molecules intercalated in MMT interlayers are shown in Fig. 3. It is worth noting that these PEG compounds exhibit different conformational characteristics owing to their molecular configurations and confinement effect. Most PEG2 molecules incline to be parallel to the clay surface with a stretched form, while PEG4 molecules tend to form a crown-like structure. Interestingly, PEG8 molecules are likely to adopt helical or coil configurations, which is also observed in previous studies of PEGs immersed in aqueous solutions in the single-wall carbon nanotubes (SWCNTs) [72]. Such structure is also in line with the hypothesis proposed by Aranda *et al.* [43]. To better illustrate the orientation properties of PEGs, we present the angle distributions [73] of PEG2 and PEG4 in Fig. 4. The details about the angle definitions are described in Figure S1. For PEG2, the angle distribution has a peak at $\sim 90^\circ$ for all concentrations, corresponding to a parallel orientation. On the other hand, for PEG4, at low concentrations, there are one peak at $\sim 90^\circ$ and two shoulders at $\sim 55^\circ$ and $\sim 125^\circ$ indicating standing (with line connecting two head C atoms parallel to the surface) and tilting orientations, respectively. As PEG4 concentration increases, the peak at $\sim 90^\circ$ gradually vanishes, while the shoulders are further shifting to two sides, indicating that most PEG4 molecules tend to orient lying (with line connecting two head C atoms perpendicular to the surface) on the surface. We also present the radius of gyration R_g [74] of various PEGs at different concentrations in Table S4. It shows that R_g of PEG8 is much smaller than the half of its stretched size, manifesting a folded conformation.

In order to further investigate the structural properties of PEGs, the number density distributions of C and O atoms in the PEG molecules for 4 wt% along the z -direction are shown in Fig. 5. Here $Z = 0$ represents

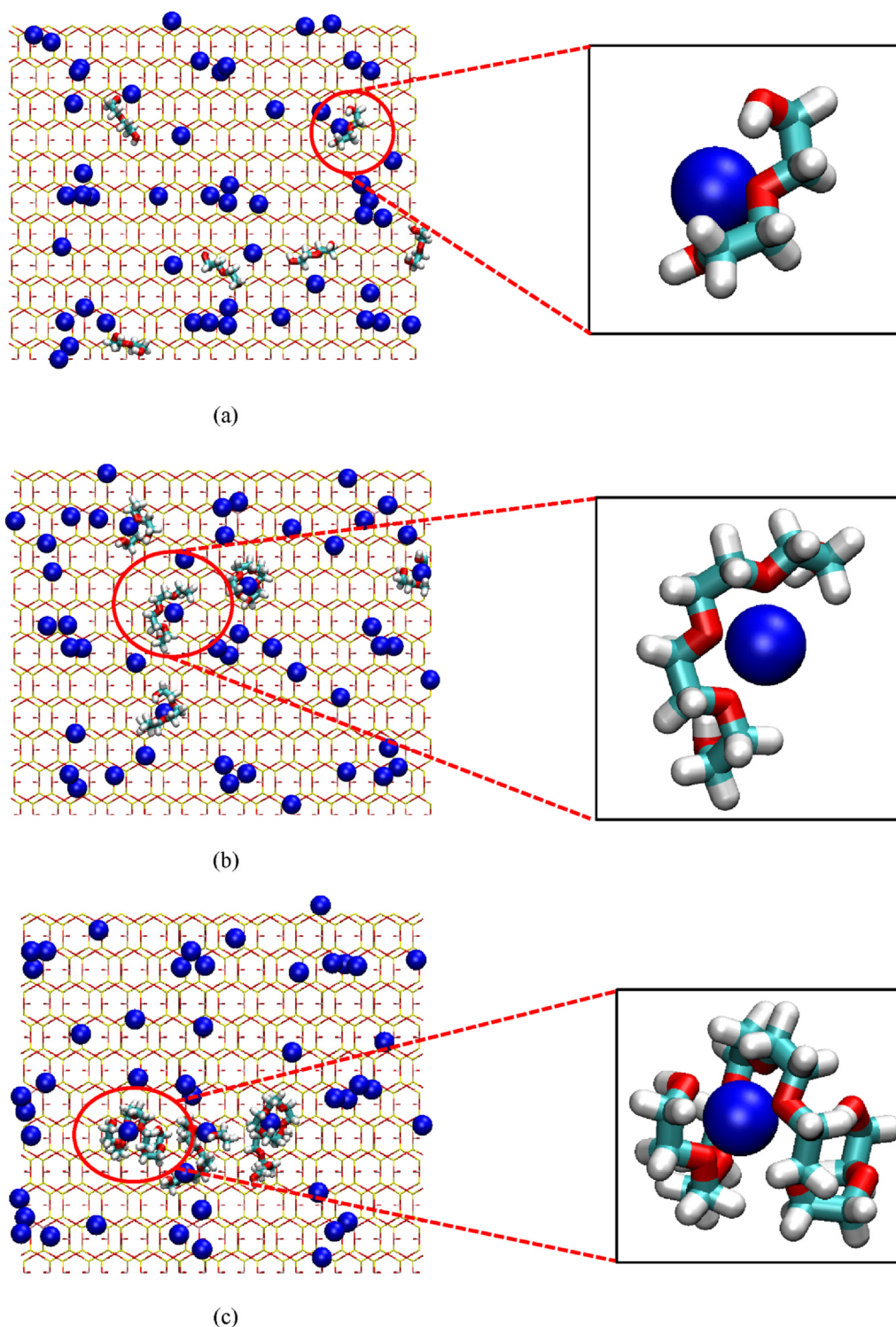


Fig. 8. Snapshots of some typical configurations of (a) PEG2; (b) PEG4; (c) PEG8 molecules with Na^+ ions. For clarity, water molecules are omitted. The color scheme is the same as in Fig. 1.

the position of outmost tetrahedral O for all the simulation system. For all PEGs, C atoms show adsorption layers near the clay surface. The peak position of C atom distributions is closer to the surface than O atoms except those belonging to $-\text{OH}$ groups (O1) in line with Su *et al.* [42]. O1 distributions show a minor shoulder close to the surface with a major peak in the middle of the pores. It is because most $-\text{OH}$ groups of PEG molecules prefer to hydrate with water or coordinate with Na^+ ions away from the pore surface, while only a small amount of $-\text{OH}$ groups form hydrogen bonds with the clay tetrahedral surface. Similar

phenomena are also observed for the cases of 8 wt% and 12 wt% as shown in Figure S2. However, for PEG4, the minor shoulder of O1 disappears at 12 wt%, which is consistent with their favorable orientation as lying on the surface.

3.1.2. Water

Number density profiles of water oxygen (Ow) and hydrogen (Hw) with varying PEG concentrations are presented in Fig. 6. The Ow shows adsorption layers in the vicinity of the surface indicating a strong

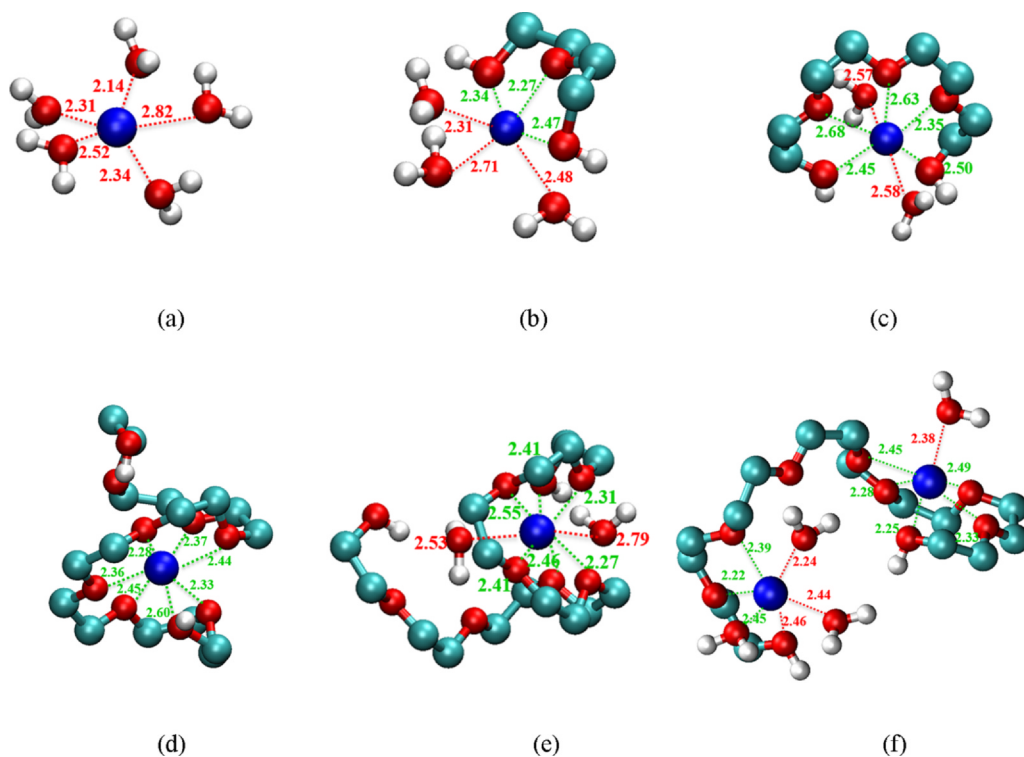


Fig. 9. Representative snapshots of various first hydration shells around Na⁺ ions. (a) Na⁺ ion purely hydrated by water for the system containing 4 wt % PEG2; (b) Na⁺ ion hydrated by water and PEG2 for the system containing 4 wt% PEG2; (c) Na⁺ ion hydrated by water and PEG4 for the system containing 4 wt% PEG4; (d ~ f) Na⁺ ions hydrated by water and PEG8 for the system containing 4 wt% PEG8. The green and red dotted lines denote the distances from Na⁺ ions to the coordinated O atoms in water and PEG molecules, respectively. The H atoms of -CH₂- groups in PEG molecules are omitted for clarity. The color scheme is the same as Fig. 1. (For interpretation of the references to color in this figure legend, the reader is referred to the web version of this article.)

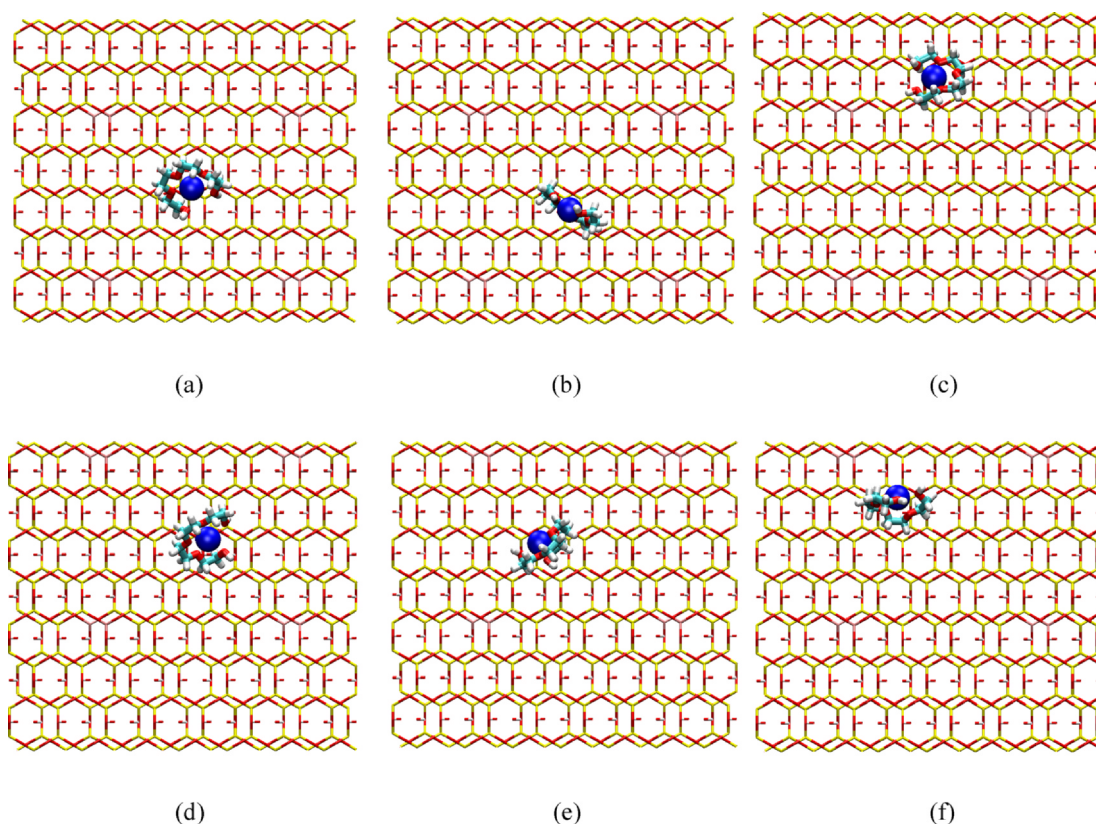


Fig. 10. Snapshots of one Na⁺-PEG4 complex at (a) $t = 20.5$ ns; (b) $t = 21$ ns; (c) $t = 21.5$ ns; (d) $t = 22$ ns; (e) $t = 22.5$ ns; (f) $t = 23$ ns.

affinity between water and clay surface. The peak value of O_w and H_w close to the surface decreases after adding PEGs, suggesting that PEGs are capable of displacing water from the pore surface in line with the previous work [37].

The orientation of water molecules can be described by the

orientation-order parameter $S(Z)$ [22,75],

$$S(Z) = 1.5 \langle \cos^2 \alpha \rangle - 0.5 \quad (3)$$

where α is the angle between the dipole moment of water molecule and the z -axis and represents the ensemble averages. If all water molecules

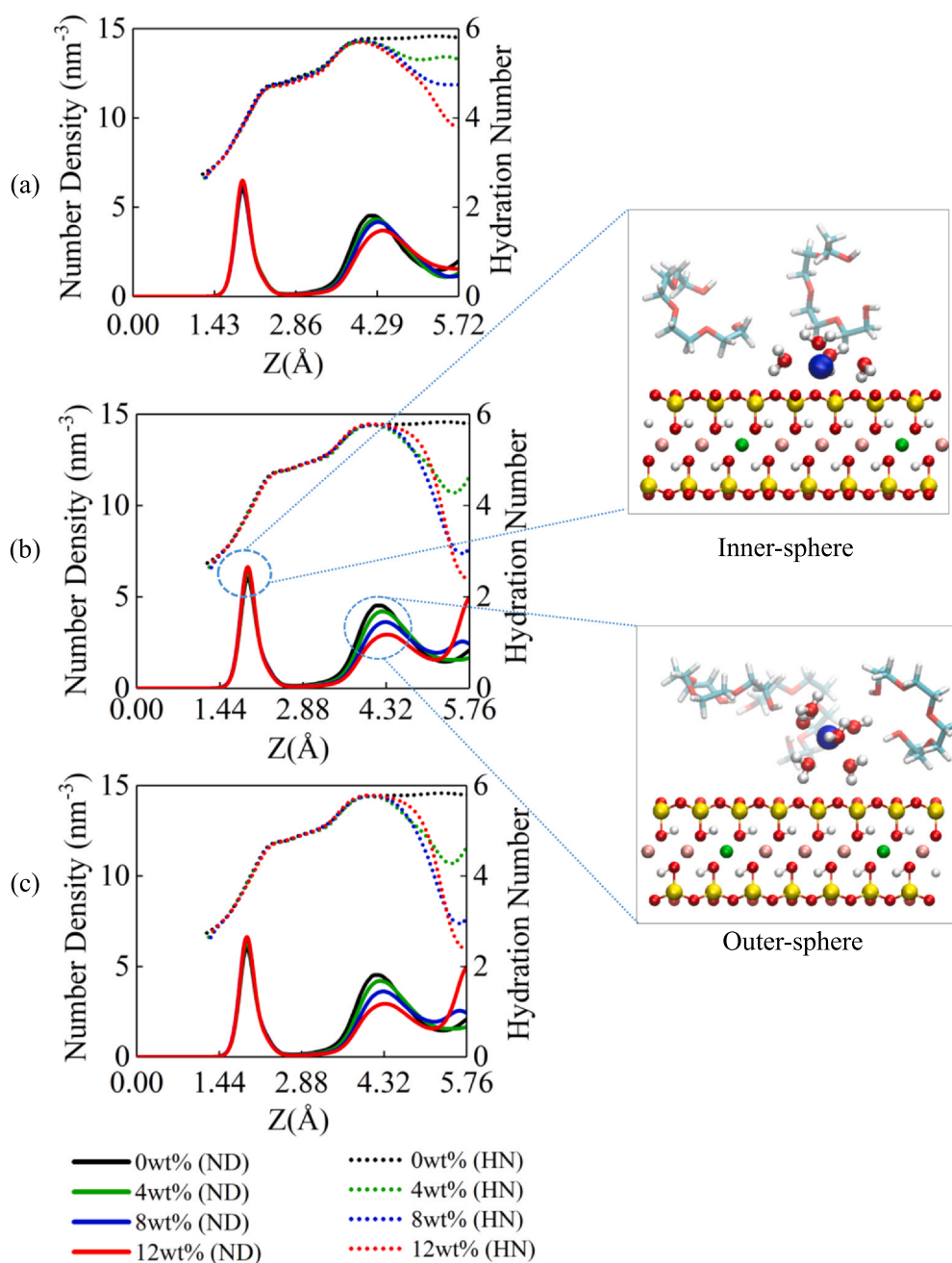


Fig. 11. Number density (ND) distributions of Na^+ ion and its hydration number (HN) distributions in the presence of (a) PEG2; (b) PEG4; (c) PEG8. We highlight the Na^+ ions hydration structures with inner-sphere (top-right) and outer-sphere (bottom-right) forms, respectively, in the presence of 12 wt% PEG4.

are perpendicular to the clay surface, $S(Z) = 1$; when they are parallel to the pore surface, $S(Z) = -0.5$; $S(Z) = 0$ represents a random orientation. Fig. 7 shows $S(Z)$ of water molecules before and after adding PEGs. In the proximity of pore surface, water molecules incline to be perpendicular to the surface while a random distribution is observed in the middle of the pores. Overall, the introduction of PEGs has little influence on the water orientation near the pore surface, while some minor changes are observed in the middle of the pores.

3.1.3. Na^+ ions

It is generally believed that the hydration of counter-ions is one of the driving forces to absorb water into the clay interlayers, which results in clay swelling. Therefore, it is crucial to investigate the effect of PEGs on the Na^+ hydration structure. The hydration behavior of Na^+ ions in the MMT interlayers can be demonstrated by the radial

distribution density (RDD) [76] and the coordination number (CN). The RDD for species B around species A in confinement space $g_{A-B}(r)$ is given as,

$$g_{A-B}(r) = \frac{1}{4\pi r^2} \frac{dN_{A-B}}{dr} \quad (4)$$

where dN_{A-B} is the average number of species B around species A between the distance of r and $r + dr$.

The CN as a function of distance r can be obtained by $g_{A-B}(r)$ [70],

$$\text{CN}(r) = 4\pi \int_0^r r'^2 g_{A-B}(r') dr' \quad (5)$$

The hydration number (HN) can be defined as the CN of O_w around Na^+ obtained from the integration shown in Eq. (5) from $r = 0$ to the first minimum after the first peak in RDD. The RDD curves for $\text{Na}^+ - \text{O}_w$ are presented in Figure S3 and the HN is listed in Table S5. The first

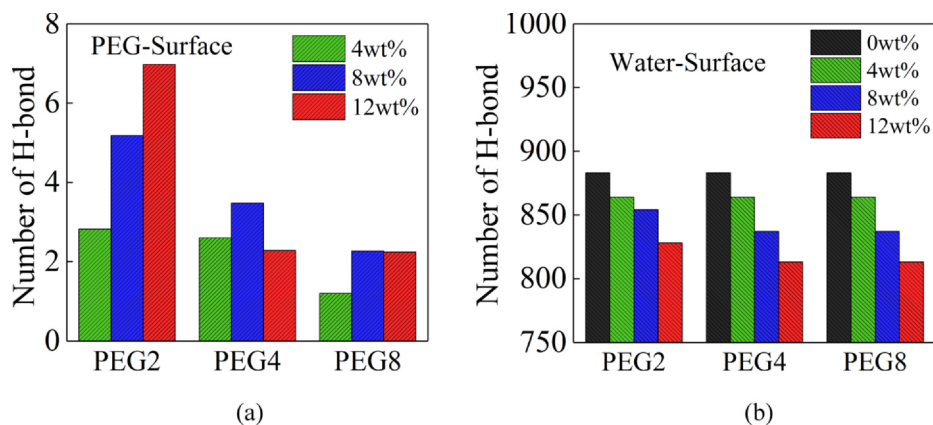


Fig. 12. The ensemble averaged total hydrogen bond number between (a) PEG and surface; (b) water and surface in the presence of various PEGs.

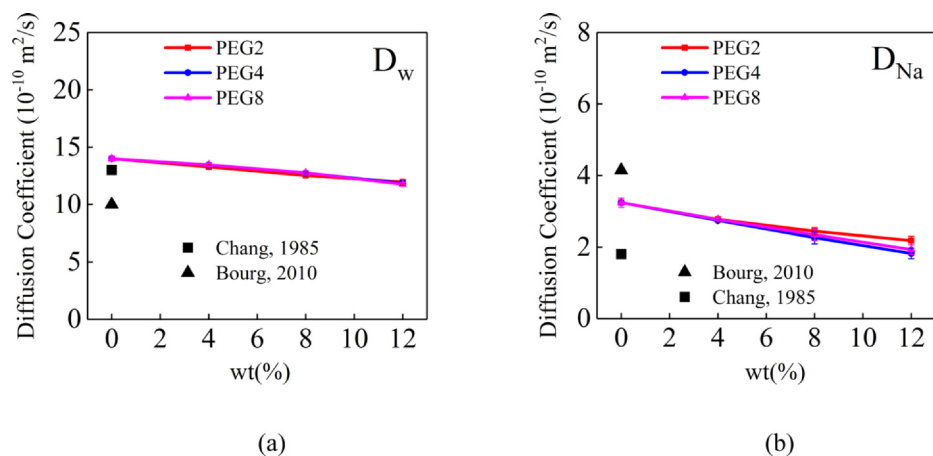


Fig. 13. The x-y plane diffusion coefficients of (a) water; (b) Na⁺ ions as a function of PEGs weight percent.

peak of Na⁺-O_w occurs at ~ 2.355 Å, which agrees well with the previous MD simulations [77,78]. For all cases, the first peak value in RDD curves decreases as PEG content increases. As a result, the HN decreases as PEG concentration increases. The smaller HN appears in the presence of PEG4 and PEG8 molecules. It is because PEG4 and PEG8 are likely to wrap Na⁺ ions and cage them inside by cutting off their connection with water molecules as shown in Fig. 8. On the other hand, for PEG2, the caging structure is not obvious. In addition, it is observed that such Na⁺-PEG complex mainly appears in the middle of the MMT interlayers as displayed in Figure S4. Similar phenomenon has been reported for PEGs interacting with K⁺ and Na⁺ ions in MMT interlayers [33,50]. However, we note that these works did not consider the presence of water, which may not conform to the realistic aqueous environment during drilling operation.

To better explain the suppressed hydration of Na⁺ ions, we present the snapshots of different hydration states of Na⁺ ions with/without PEGs in MMT interlayers in Fig. 9. In general, Na⁺ ions tend to be hydrated by five water molecules, if not wrapped by PEGs. The number of water molecules in the first hydration shell of Na⁺ ion drastically declines, once Na⁺ ion is wrapped by PEG molecules. It should be noted that PEG8 can chelate with one or two Na⁺ ions, while PEG2 and PEG4 generally can only coordinate with one Na⁺ ion. In addition, PEG8 is capable of forming a helical cage fully coating Na⁺ ions to further reduce their HN.

To illustrate the stability of Na⁺-PEG complex, in Fig. 10, we present the snapshots of dynamic evolution for one Na⁺-PEG4 complex from 20 ns to 23 ns (A video is available as the [supplementary material](#)). This Na⁺-PEG4 complex moves as a whole, indicating a high stability. A similar phenomenon observed for Na⁺-PEG8 complex is

presented in Figure S5. While PEG8 can accommodate two Na⁺ ions, one of them may escape from the caging during the process. In contrast, PEG2 cannot form a stable Na⁺-PEG2 complex.

To better understand the effect of PEGs on Na⁺ ion hydration in different regions, in Fig. 11, we show the number density distributions of Na⁺ ion and its HN distributions for various PEG concentrations. Na⁺ ions form both inner- and outer-sphere surface complexes in the MMT interlayers, in an agreement with the earlier simulation works [48,79]. As PEG amount increases, the peak value of Na⁺ ion distribution near the pore surface slightly increases as some water molecules on the surface are depleted. The second peak in Na⁺ ion distribution drastically decreases, as PEG concentration increases. For 12 wt% PEG4 and PEG8, Na⁺ ions accumulate in the middle of the pores. It is probably because PEG4 and PEG8 can wrap and cage Na⁺ ions as shown in Fig. 8, while such Na⁺-PEG4 and Na⁺-PEG8 complexes mainly form in the middle of the pores. Close to the pore surface, Na⁺ ions form inner-sphere structure, which can only coordinate with water molecules in a hemisphere shell, while those away from the pore surface can form out-sphere structure coordinating with water molecules in a spherical shell. The HN of Na⁺ ion in the second peak of its distributions is about two times of that in the first peak. In the presence of PEGs, HN of Na⁺ ion drastically decreases in the middle of the pores while those in other regions remain the same. It is due to the formation of Na⁺-PEG complexes. In contrast to PEG2, PEG4 and PEG8 are capable of forming more stable Na⁺-PEG complexes which can drastically reduce the hydration of Na⁺ ions as shown in Fig. 9. As there are more Na⁺ ions with a lower hydration number in the middle of the MMT interlayers in the presence of PEG4 and PEG8, the average hydration number of Na⁺ ions after adding PEG4 and PEG8 is lower as shown in

Table S5.

3.2. Hydrogen bond

MMT has a high propensity to absorb water by forming hydrogen bonding between water and aluminate and silicate groups of the substrates [31]. It is assumed that PEG molecules can form hydrogen bonds with tetrahedral sheets disrupting the hydrogen bonding network formed between water molecules and clay surface. Thus, it is important to investigate the hydrogen bonds between PEG and clay surface and the change in the hydrogen bonding number between water and surface after adding PEG. In this work, the hydrogen bonds are identified using a geometrical criterion, according to which a hydrogen bond is determined if $r_{O\cdots H} < 3.5 \text{ \AA}$ and $\angle O\cdots O-H \leq 30^\circ$ [80]. The ensemble averaged total hydrogen bonding number between PEG and surface and that between water and surface is shown in Fig. 12. All PEGs can form hydrogen bonds with the MMT surface. The total hydrogen bond number between PEG2 and surface increases as PEG2 concentration increases. On the other hand, for PEG4 and PEG8, the total hydrogen bond number between PEG and surface shows a non-monotonic behavior with their concentration. It is probably because PEG4 and PEG8 can form Na^+ -PEG4 and Na^+ -PEG8 complexes, respectively, while these complexes mainly form in the middle of the pores. The total hydrogen bond number between PEG4 and surface is slightly smaller than that of PEG2 at 4 wt%, while the number of PEG2 molecules in the MMT interlayers is almost two times of that of PEG4. As shown in Fig. 4, PEG4 has a higher propensity to stand on the surface at 4 wt%, which is favorable to form hydrogen bonds with pore surface. In addition, as shown in Fig. 5, PEG2 and PEG4 O1 distributions on the pore surface are comparable. As shown in Fig. 4, as PEG4 concentration increases, they tend to take the tilting configuration which has a lower hydrogen bonding number between PEG4 and surface than the standing one. On the other hand, as water molecules are depleted from the pore surface due to the introduction of PEG molecules, the total hydrogen bond number between water and surface gradually decreases as PEG concentration increases.

3.3. Diffusion coefficients

The x - y plane diffusion coefficients are estimated from the slope of the mean square displacements of the water and Na^+ ions versus time, which are presented in Table S6. To get a better understanding of the effect of PEGs on the mobility of water and Na^+ ions, the diffusion coefficient variation as a function of PEG concentration are shown in Fig. 13. The calculated diffusion coefficients of Na^+ ions and water without PEGs are in a reasonable agreement with the previous simulation results [2,81]. Generally, water diffusion coefficient drops linearly as PEG concentration increases, while the effect of PEG types is negligible. It is because the introduction of PEGs increases fluid viscosity. On the other hand, for Na^+ ion, while the diffusion coefficient decreases due to the presence of PEGs, PEG4 has a more pronounced effect than PEG8, and then followed by PEG2. It is probably due to the formation of Na^+ -PEGs complexes, which significantly limits Na^+ ion mobility. PEG4 and PEG8 can form a caging structure to wrap Na^+ inside, which can be quite stable as shown in Fig. 10. While molecular weight of PEG8 is almost twice of that of PEG4, the PEG8 cannot always wrap two Na^+ ions inside. Therefore, Na^+ ion mobility is slightly higher in the presence of PEG8 than that of PEG4 at the same PEG weight percent. We also present the diffusion coefficients in the x - and y - directions in Figure S6. It shows that the diffusion coefficients are isotropic in the x - and y - directions.

4. Conclusion

In this work, we used MD simulations to study the structural and dynamic properties of water, Na^+ ions and PEGs with varying chain

length and concentration in MMT interlayers. We found that PEGs with varying chain length exhibit diverse configurations when intercalating into the MMT interlayer. PEG2 have a propensity to distribute parallel to the surface, while PEG4 and PEG8 molecules incline to form a crown-like or coil structure. In the presence of PEG4 and PEG8, Na^+ caging mainly occurs in the middle of the MMT interlayers, which significantly reduces the hydration ability of Na^+ , while Na^+ hydration is nearly unaffected close to the pore surface. We also found that PEGs can displace water molecules from the pore surface, forming hydrogen bonding with the pore surface. As a result, the hydrogen bonding number between water and pore surface decreases due to the introduction of PEGs. However, PEGs have a negligible effect on the orientation of water molecules on the pores surface. Furthermore, the formation of Na^+ -PEG4 and Na^+ -PEG8 complexes can greatly reduce Na^+ ion mobility. Our work systematically studied the structural and dynamic properties of MMT interlayer species and may provide important insights into the clay swelling inhibition mechanisms and rational design of high-performance water-based drilling fluid additives.

CRedit authorship contribution statement

Mingshan Zhang: Methodology, Software, Validation, Formal analysis, Investigation, Writing - original draft, Writing - review & editing, Visualization. **Hui Mao:** Methodology, Writing - review & editing, Supervision, Funding acquisition. **Zhehui Jin:** Conceptualization, Formal analysis, Investigation, Resources, Writing - review & editing, Supervision, Funding acquisition.

Declaration of Competing Interest

The authors declare that they have no known competing financial interests or personal relationships that could have appeared to influence the work reported in this paper.

Acknowledgement

The authors acknowledge China Scholarship Council (CSC) for financial support provided to M. Zhang. This work is supported partly by the Open Fund (PLC20180704) of the State Key Laboratory of Oil and Gas Reservoir Geology and Exploitation (Chengdu University of Technology) (H. Mao). This research was enabled in part by support provided by Westgrid (www.westgrid.ca) and Compute Canada (www.computeCanada.ca). Z. Jin also greatly acknowledges a Discovery Grant from Natural Sciences and Engineering Research Council of Canada (NSERC RGPIN-2017-05080).

Appendix A. Supplementary data

Supplementary data to this article can be found online at <https://doi.org/10.1016/j.apsusc.2020.147700>.

References

- [1] R.T. Cygan, J.A. Greathouse, H. Heinz, A.G. Kalinichev, Molecular models and simulations of layered materials, *J. Mater. Chem.* 19 (2009) 2470–2481.
- [2] S.C. Aboudi Mana, M.M. Hanafiah, A.J.K. Chowdhury, Environmental characteristics of clay and clay-based minerals, *Geol. Ecol. Landscapes* 1 (2017) 155–161.
- [3] S. Assemi, H. Erten, Sorption of radioiodine on organic rich soil, clay minerals and alumina, *J. Radioanal. Nucl. Chem.* 178 (1994) 193–204.
- [4] M.E. Parolo, G.R. Pettinari, T.B. Musso, M.P. Sánchez-Izquierdo, L.G. Fernández, Characterization of organo-modified bentonite sorbents: The effect of modification conditions on adsorption performance, *Appl. Surf. Sci.* 320 (2014) 356–363.
- [5] A. Gładysz-Plaska, M. Majdan, S. Pikus, D. Sternik, Simultaneous adsorption of chromium (VI) and phenol on natural red clay modified by HDTMA, *Chem. Eng. J.* 179 (2012) 140–150.
- [6] W. Somerton, C. Radke, Role of clays in the enhanced recovery of petroleum from some California sands, *J. Petrol. Technol.* 35 (1983) 643–654.
- [7] M. Ejder-Korucu, A. Gürses, S. Karaca, Poly (ethylene oxide)/clay nanocomposites: thermal and mechanical properties, *Appl. Surf. Sci.* 378 (2016) 1–7.

- [8] S. Zhu, J. Chen, H. Li, Y. Cao, Structure and conformation of poly (ethylene glycol) in confined space of montmorillonite, *Appl. Surf. Sci.* 264 (2013) 500–506.
- [9] J. Wu, M.M. Lerner, Structural, thermal, and electrical characterization of layered nanocomposites derived from sodium-montmorillonite and polyethers, *Chem. Mater.* 5 (1993) 835–838.
- [10] H. Schott, Interaction of nonionic detergents and swelling clays, *Kolloid-Zeitschrift und Zeitschrift für Polymere* 199 (1964) 158–169.
- [11] S. Gou, T. Yin, Q. Xia, Q. Guo, Biodegradable polyethylene glycol-based ionic liquids for effective inhibition of shale hydration, *RSC Adv.* 5 (2015) 32064–32071.
- [12] A. Alemdar, N. Güngör, O. Ece, O. Atici, The rheological properties and characterization of bentonite dispersions in the presence of non-ionic polymer PEG, *J. Mater. Sci.* 40 (2005) 171–177.
- [13] M. Ghasemi, A. Moslemizadeh, K. Shahbazi, O. Mohammadzadeh, S. Zendejboudi, S. Jafari, Primary evaluation of a natural surfactant for inhibiting clay swelling, *J. Pet. Sci. Eng.* 178 (2019) 878–891.
- [14] G. Xie, P. Luo, M. Deng, J. Su, Z. Wang, R. Gong, J. Xie, S. Deng, Q. Duan, Intercalation behavior of branched polyethyleneimine into sodium bentonite and its effect on rheological properties, *Appl. Clay Sci.* 141 (2017) 95–103.
- [15] S. Villabona-Estupiñán, J. de Almeida Rodrigues, R.S.V. Nascimento, Understanding the clay-PEG (and hydrophobic derivatives) interactions and their effect on clay hydration and dispersion: a comparative study, *Appl. Clay Sci.* 143 (2017) 89–100.
- [16] H.M. Ahmed, M.S. Kamal, M. Al-Harthi, Polymeric and low molecular weight shale inhibitors: a review, *Fuel* 251 (2019) 187–217.
- [17] H. Zhong, Z. Qiu, W. Huang, D. Sun, D. Zhang, J. Cao, Synergistic stabilization of shale by a mixture of polyamidamine dendrimers modified bentonite with various generations in water-based drilling fluid, *Appl. Clay Sci.* 114 (2015) 359–369.
- [18] S.B. Hamed, M. Belhadri, Rheological properties of biopolymers drilling fluids, *J. Pet. Sci. Eng.* 67 (2009) 84–90.
- [19] E. Van Oort, On the physical and chemical stability of shales, *J. Pet. Sci. Eng.* 38 (2003) 213–235.
- [20] C. Thaumitz, A. Patel, G. Coffin, L. Conn, New environmentally safe high-temperature water-based drilling-fluid system, *SPE Drill. Complet* 14 (1999) 185–189.
- [21] J.P. Deville, B. Fritz, M. Jarrett, Development of water-based drilling fluids customized for shale reservoirs, *SPE Drill. Complet* 26 (2011) 484–491.
- [22] Z. Jin, A. Firoozabadi, Methane and carbon dioxide adsorption in clay-like slit pores by Monte Carlo simulations, *Fluid Phase Equilib.* 360 (2013) 456–465.
- [23] C.T. Chiou, D.W. Rutherford, Effects of exchanged cation and layer charge on the sorption of water and EGME vapors on montmorillonite clays, *Clays Clay Miner.* 45 (1997) 867–880.
- [24] E. Hensen, T. Tambach, A. Blik, B. Smit, Adsorption isotherms of water in Li-, Na-, and K-montmorillonite by molecular simulation, *J. Chem. Phys.* 115 (2001) 3322–3329.
- [25] M. Chávez-Páez, K. Van Workum, L. De Pablo, J.J. de Pablo, Monte Carlo simulations of Wyoming sodium montmorillonite hydrates, *J. Chem. Phys.* 114 (2001) 1405–1413.
- [26] M. Fu, Z. Zhang, P. Low, Changes in the properties of a montmorillonite-water system during the adsorption and desorption of water: hysteresis, *Clays Clay Miner.* 38 (1990) 485–492.
- [27] J. Odom, P. Low, A kinetic method for determining desorption isotherms of water on clays 1, *Soil Sci. Soc. Am. J.* 47 (1983) 1039–1041.
- [28] G. Sposito, R. Prost, Structure of water adsorbed on smectites, *Chem. Rev.* 82 (1982) 553–573.
- [29] A. Bains, E. Boek, P. Coveney, S. Williams, M. Akbar, Molecular modelling of the mechanism of action of organic clay-swelling inhibitors, *Mol. Simul.* 26 (2001) 101–145.
- [30] R. Anderson, I. Ratcliffe, H. Greenwell, P. Williams, S. Cliffe, P. Coveney, Clay swelling—a challenge in the oilfield, *Earth Sci. Rev.* 98 (2010) 201–216.
- [31] R. Gholami, H. Elochukwu, N. Fakhari, M. Sarmadivaleh, A review on borehole instability in active shale formations: interactions, mechanisms and inhibitors, *Earth Sci. Rev.* 177 (2018) 2–13.
- [32] J.L. Suter, L. Kabanal, M. Khader, P.V. Coveney, Ab initio molecular dynamics study of the interlayer and micropore structure of aqueous montmorillonite clays, *Geochim. Cosmochim. Acta* 169 (2015) 17–29.
- [33] J.L. Suter, P.V. Coveney, R.L. Anderson, H.C. Greenwell, S. Cliffe, Rule based design of clay-swelling inhibitors, *Energy Environ. Sci.*, 4 4572.
- [34] J. Ulbricht, R. Jordan, R. Luxenhofer, On the biodegradability of polyethylene glycol, polypeptides and poly (2-oxazoline) s, *Biomaterials* 35 (2014) 4848–4861.
- [35] R. Parfitt, D. Greenland, The adsorption of poly (ethylene glycols) on clay minerals, *Clay Min.* 8 (1970) 305–315.
- [36] B. Bloys, N. Davis, B. Smolen, L. Bailey, O. Houwen, P. Reid, J. Sherwood, L. Fraser, M. Hodder, F. Montrouge, Designing and managing drilling fluid, *Oilfield Rev.* 6 (1994) 33–43.
- [37] M. Aston, G. Elliott, Water-based glycol drilling muds: shale inhibition mechanisms, in: *European Petroleum Conference, Society of Petroleum Engineers*, 1994.
- [38] X. Zhao, K. Urano, S. Ogasawara, Adsorption of polyethylene glycol from aqueous solution on montmorillonite clays, *Colloid Polym. Sci.* 267 (1989) 899–906.
- [39] P. Reid, B. Dolan, S. Cliffe, Mechanism of shale inhibition by polyols in water based drilling fluids, in: *SPE International Symposium on Oilfield Chemistry, Society of Petroleum Engineers*, 1995.
- [40] C.E.C. De Souza, A.S. Lima, R.S.V. Nascimento, Hydrophobically modified poly (ethylene glycol) as reactive clays inhibitor additive in water-based drilling fluids, *J. Appl. Polym. Sci.* 117 (2010) 857–864.
- [41] R. Mosser-Ruck, K. Devineau, D. Charpentier, M. Cathelineau, Effects of ethylene glycol saturation protocols on XRD patterns: a critical review and discussion, *Clays Clay Miner.* 53 (2005) 631–638.
- [42] C.-C. Su, Y.-H. Shen, Effects of poly (ethylene oxide) adsorption on the dispersion of smectites, *Colloids Surf., A* 312 (2008) 1–6.
- [43] P. Aranda, E. Ruiz-Hitzky, Poly (ethylene oxide)-silicate intercalation materials, *Chem. Mater.* 4 (1992) 1395–1403.
- [44] S. Zhan, Y. Su, Z. Jin, W. Wang, L. Li, Effect of water film on oil flow in quartz nanopores from molecular perspectives, *Fuel* 262 (2020) 116560.
- [45] N.T. Skipper, F.-R.C. Chang, G. Sposito, Monte Carlo simulation of interlayer molecular structure in swelling clay minerals. 1. Methodology, *Clays Clay Miner.* 43 (1995) 285–293.
- [46] J.A. Greathouse, R.T. Cygan, J.T. Fredrich, G.R. Jerauld, Molecular dynamics simulation of diffusion and electrical conductivity in montmorillonite interlayers, *Phys. Chem. C* 120 (2016) 1640–1649.
- [47] B. Rotenberg, V. Marry, R. Vuilleumier, N. Malikova, C. Simon, P. Turq, Water and ions in clays: Unraveling the interlayer/micropore exchange using molecular dynamics, *Geochim. Cosmochim. Acta* 71 (2007) 5089–5101.
- [48] Y. Liu, X. Ma, H.A. Li, J. Hou, Competitive adsorption behavior of hydrocarbon (s)/CO₂ mixtures in a double-nanopore system using molecular simulations, *Fuel* 252 (2019) 612–621.
- [49] R.L. Anderson, H.C. Greenwell, J.L. Suter, R.M. Jarvis, P.V. Coveney, Towards the design of new and improved drilling fluid additives using molecular dynamics simulations, *Anais da Academia Brasileira de Ciências* 82 (2010) 43–60.
- [50] M. Krishnan, M. Saharay, R.J. Kirkpatrick, Molecular dynamics modeling of CO₂ and poly (ethylene glycol) in montmorillonite: The structure of clay-polymer composites and the incorporation of CO₂, *Phys. Chem. C* 117 (2013) 20592–20609.
- [51] M. Szczerba, A.G. Kalinichev, Intercalation of ethylene glycol in smectites: Several molecular simulation models verified by X-ray diffraction data, *Clays Clay Miner.* 64 (2016) 488–502.
- [52] Q. Zeng, A. Yu, G. Lu, R. Standish, Molecular dynamics simulation of organic-inorganic nanocomposites: layering behavior and interlayer structure of organoclays, *Chem. Mater.* 15 (2003) 4732–4738.
- [53] S. Basfar, A. Mohamed, S. Elkhatatny, A. Al-Majed, A combined barite-ilmenite weighting material to prevent barite sag in water-based drilling fluid, *Materials* 12 (2019) 1945.
- [54] S. Plimpton, Fast parallel algorithms for short-range molecular dynamics, *Sandia National Labs, Albuquerque, NM (United States)*, 1993.
- [55] R.T. Cygan, J.-J. Liang, A.G. Kalinichev, Molecular models of hydroxide, oxyhydroxide, and clay phases and the development of a general force field, *Phys. Chem. B* 108 (2004) 1255–1266.
- [56] H. Berendsen, J. Grigera, T. Straatsma, The missing term in effective pair potentials, *J. Phys. Chem.* 91 (1987) 6269–6271.
- [57] D.E. Smith, L.X. Dang, Computer simulations of NaCl association in polarizable water, *J. Chem. Phys.* 100 (1994) 3757–3766.
- [58] W.L. Jorgensen, D.S. Maxwell, J. Tirado-Rives, Development and testing of the OPLS all-atom force field on conformational energetics and properties of organic liquids, *J. Am. Chem. Soc.* 118 (1996) 11225–11236.
- [59] B. Schampera, R. Solc, S. Woche, R. Mikutta, S. Dultz, G. Guggenberger, D. Tunega, Surface structure of organoclays as examined by X-ray photoelectron spectroscopy and molecular dynamics simulations, *Clay Min.* 50 (2015) 353–367.
- [60] B. Fazelabdolabadi, A. Alizadeh-Mojarad, A molecular dynamics investigation into the adsorption behavior inside 001 kaolinite and 1014 calcite nano-scale channels: the case with confined hydrocarbon liquid, acid gases, and water, *Appl. Nanosci.* 7 (2017) 155–165.
- [61] R.-G. Xu, Y. Leng, Squeezing and stick-slip friction behaviors of lubricants in boundary lubrication, *Proc. Natl. Acad. Sci.* 115 (2018) 6560–6565.
- [62] H. Lorentz, Ueber die Anwendung des Satzes vom Virial in der kinetischen Theorie der Gase, *Ann. Phys.* 248 (1881) 127–136.
- [63] R.W. Hockney, J.W. Eastwood, *Computer Simulation using Particles*, crc Press, 1988.
- [64] E. Ferrage, B. Lanson, B.A. Sakharov, V.A. Drits, Investigation of smectite hydration properties by modeling experimental X-ray diffraction patterns: Part I. Montmorillonite hydration properties, *Am. Miner.* 90 (2005) 1358–1374.
- [65] R. Mooney, A. Keenan, L. Wood, Adsorption of water vapor by montmorillonite. II. Effect of exchangeable ions and lattice swelling as measured by X-ray diffraction, *J. Am. Chem. Soc.* 74 (1952) 1371–1374.
- [66] K. Tamura, H. Yamada, H. Nakazawa, Stepwise hydration of high-quality synthetic smectite with various cations, *Clays Clay Miner.* 48 (2000) 400–404.
- [67] W. Humphrey, A. Dalke, K. Schulten, VMD: visual molecular dynamics, *J. Mol. Graph.* 14 (1996) 33–38.
- [68] D.J. Evans, B.L. Holian, The nose–hoover thermostat, *J. Chem. Phys.* 83 (1985) 4069–4074.
- [69] M. Tuckerman, B.J. Berne, G.J. Martyna, Reversible multiple time scale molecular dynamics, *J. Chem. Phys.* 97 (1992) 1990–2001.
- [70] D. Frenkel, B. Smit, *Understanding Molecular Simulation: From Algorithms to Applications*, second ed., Elsevier, Cambridge, 2002.
- [71] I.C. Bourg, G. Sposito, Connecting the molecular scale to the continuum scale for diffusion processes in smectite-rich porous media, *Environ. Sci. Technol.* 44 (2010) 2085–2091.
- [72] U.R. Dahal, E.E. Dormidontova, Spontaneous insertion, helix formation, and hydration of polyethylene oxide in carbon nanotubes, *Phys. Rev. Lett.* 117 (2016) 027801.
- [73] N. Skipper, G. Sposito, F.-R.C. Chang, Monte Carlo simulation of interlayer molecular structure in swelling clay minerals. 2. Monolayer hydrates, *Clays Clay Miner.* 43 (1995) 294–303.
- [74] R. Stepto, T. Chang, P. Kratochvíl, M. Hess, K. Horie, T. Sato, J. Vohlřídál, Definitions of terms relating to individual macromolecules, macromolecular assemblies, polymer solutions, and amorphous bulk polymers (IUPAC Recommendations 2014), *Pure Appl. Chem.* 87 (2015) 71–120.

- [75] I. Bitsanis, G. Hadziioannou, Molecular dynamics simulations of the structure and dynamics of confined polymer melts, *J. Chem. Phys.* 92 (1990) 3827–3847.
- [76] Y. Nan, W. Li, Z. Jin, Role of alcohol as a cosurfactant at the brine-oil interface under a typical reservoir condition, *Langmuir* 36 (2020) 5198–5207.
- [77] L. Zhang, X. Lu, X. Liu, J. Zhou, H. Zhou, Hydration and mobility of interlayer ions of (Na_x, Ca_y)-montmorillonite: a molecular dynamics study, *Phys. Chem. C* 118 (2014) 29811–29821.
- [78] S.B. Rempe, L.R. Pratt, G. Hummer, J.D. Kress, R.L. Martin, A. Redondo, The hydration number of Li⁺ in liquid water, *J. Am. Chem. Soc.* 122 (2000) 966–967.
- [79] E. Boek, P. Coveney, N. Skipper, Monte Carlo molecular modeling studies of hydrated Li-, Na-, and K-smectites: understanding the role of potassium as a clay swelling inhibitor, *J. Am. Chem. Soc.* 117 (1995) 12608–12617.
- [80] R. Kumar, J. Schmidt, J. Skinner, Hydrogen bonding definitions and dynamics in liquid water, *J. Chem. Phys.* 126 (2007) 05B611.
- [81] F.-R.C. Chang, N. Skipper, G. Sposito, Computer simulation of interlayer molecular structure in sodium montmorillonite hydrates, *Langmuir* 11 (1995) 2734–2741.